Available online at www.sciencedirect.com
SCIENCE DIRECT®
ELSEVIER
International Journal of Solids and Structures 43 (2006) 2174–2192
INTERNATIONAL JOURNAL OF SOLIDS and STRUCTURES
www.elsevier.com/locate/ijsolstr

Finite element analysis for steady-state hydride-induced fracture in metals by composite model

J.L. Feng [a,*], A.G. Varias [b], Y.K. Sui [a]

[a] *Department of Engineering Mechanics, Beijing University of Technology, Pingleyuan 100, Beijing 100022, PR China*
[b] *Materials Science, Technology and Society, Malmö University, SE-205 06 Malmö, Sweden*

Received 20 December 2004; received in revised form 30 April 2005
Available online 24 June 2005

Abstract

Delayed hydride cracking, which is observed in hydride-forming metals, due to the precipitation of hydrides near the crack tip, is investigated under conditions of constant temperature and crack velocity, plane strain and small-scale hydride-precipitation. The coupling of the operating physical processes of hydrogen-diffusion, hydride precipitation and material deformation is taken into account. The material is assumed to be an elastic composite made of hydrides and solid solution, with properties depending locally on the volume fraction of the hydrides. In the present analysis, the composite elastic properties have been derived by a generalized self consistent model for particulate composites. With respect to hydride-precipitation, two cases have been considered: (i) precipitation in a homogeneous medium with elastic properties, equal to the effective properties of the composite and (ii) precipitation in an inhomogeneous medium, where the expanding hydride has different elastic properties than those of the surrounding solid solution. The differences between the near-tip field distributions, produced by the two precipitation models, are relatively small. The effect of the hydrogen concentration far from the crack tip, on the near-tip field is also studied. It is shown that for small crack growth velocities, near the threshold stress intensity factor, the remote hydrogen concentration weakly affects the normalized stress distribution in the hydride-precipitation zone, which is controlled by the thermodynamically required hydrostatic stress, under hydrogen chemical equilibrium. However, for values of the applied stress intensity factor and the crack tip velocity, away from the threshold stress intensity factor and crack arrest, the effect of remote hydrogen concentration on the normalized near-tip stress field is strong. Reduction of the remote hydrogen concentration generally leads to reduction of the hydride-precipitation zone and increase of the near-tip stresses. Also reduction of the remote hydrogen concentration leads to distributions closer to those under hydrogen chemical equilibrium.

Keywords: Hydride; Hydrogen; Delayed hydride cracking; Crack growth

* Corresponding author. Tel.: +86 10 67392760; fax: +86 10 67391617.
E-mail address: jili.feng@bjut.edu.cn (J.L. Feng).

0020-7683/$ - see front matter © 2005 Elsevier Ltd. All rights reserved.
doi:10.1016/j.ijsolstr.2005.05.001

1. Introduction

Delayed hydride cracking is a sub-critical crack growth mechanism, according to which a crack propagates in a hydride forming metal, such as zirconium, due to the precipitation and fracture of hydrides at the tip. Extensive review on hydride-induced embrittlement, in the case of zirconium alloys, is given by Northwood and Kosasih (1983). The interested reader can also refer to the Ph.D. thesis by Efsing (1998).

With respect to the simulation of delayed hydride cracking, an important issue is the coupling of the operating physical mechanisms of hydrogen diffusion, hydride-precipitation, non-mechanical energy flow (mainly in the case of temperature gradients) and material deformation (see Soforonis, 2001; Taha and Soforonis, 2001). Varias and Massih (2002) provide detailed information on approaching the general transient problem of hydride-induced material deterioration and fracture.

In the case of stationary cracks and constant temperature, Lufrano et al. (1996, 1998) developed the first numerical models of hydride-induced embrittlement, which take into account the coupling of the operating processes. Temperature variations and crack growth initiation were considered, for the first time, coupled together with hydrogen-diffusion, hydride-precipitation and material deformation, by Varias (1998) and Varias and Massih (2000, 2002). Serebrinsky et al. (2004) recently proposed a model of hydrogen embrittlement, which takes into account the effect of the following parameters: yield strength, stress intensity factor, hydrogen concentration in the environment, and temperature.

Varias (2003a,b) extended the previous studies by considering hydride-induced steady-state crack growth, under small scale hydride precipitation and yielding, at constant temperature. It was shown that the near-tip field, when the quantities are appropriately normalized, depends on a normalized stress intensity factor, which incorporates both effects of the applied stress intensity factor and the crack velocity. It was also shown that, as the crack velocity tends to zero and the threshold stress intensity factor is approached, a hydrostatic stress plateau develops in the area of hydride-precipitation near the tip. The plateau is a result of approaching hydrogen chemical equilibrium in the solid solution. The plateau hydrostatic stress depends strongly on the remote hydrogen concentration. The same hydrostatic stress develops also behind the crack tip in the presence of hydrides.

Varias and Feng (2004a,b) continued the steady-state crack growth studies, by considering the effect of temperature and solid solution yield stress as well as the effect of different hydride and solid solution elastic properties. In their work, the terminal solid solubility of hydrogen in a stressed metal was derived analytically for hydrides with different elastic properties from those of the solid solution, irrespectively of their shape. It was confirmed, that, even under different hydride and solid solution elastic properties, a hydrostatic stress plateau develops near the crack-tip in the hydride precipitation zone, when hydrogen chemical equilibrium is approached. The plateau level is in agreement with previous predictions, based on identical hydride and solid solution elastic moduli (Varias, 2003a,b). It was also shown that at relatively small crack tip velocities, the stress distribution, when appropriately normalized, does not depend on temperature and yield stress, except in an area, very close to the crack tip, where the hydride volume fraction is large.

The present work presents more information on modeling hydride-induced steady-crack growth, by considering different hydride and solid solution elastic properties. In other words, interaction energy due to modulus difference between hydride and solid solution must critically be taken into account even within elastic field. An important element of the simulation is the calculation of the effective elastic properties of the hydride/solid-solution composite, which depend on the distribution of the hydrides in the solid and consequently on the distribution of hydride volume fraction, ahead of the propagating crack. For this purpose the theories on the mechanics of composite material are employed. There are numerous contributions to this subject that is a problem of long-standing interest for physicists and mechanicians, and the reader is referred to specialized publications (e.g. Christensen, 1979). Important and early contributions, on the determination of the effective elastic properties of composites, were given by Hashin (1962), Hill (1965) and Budiansky (1965). Recently, another expression for the effective elastic properties of composites,

whose tensor coefficients are integrals involving some of correlation functions on that characterize the structure, was presented by Torquato (1997).

In the present study, the effective elastic properties are calculated, by using the generalized self-consistent model (e.g. Christensen, 1990), called also the three-phase model. This model shows very good behavior in the full range of the volume fraction of the inclusions as well as for significantly different inclusion and matrix stiffness. Both characteristics are very useful in the present application, where the hydrides are very stiff compared to the solid solution and the hydride volume fraction tends to 1, as the crack tip is approached. According to the generalized self-consistent model, a spherical inclusion is embedded in a concentric spherical annulus of the matrix material of the prescribed volume fraction, which in turn is embedded in a infinite medium possessing the effective properties of the composite. This approach was, initially, considered, by Kerner (1956) and Van der Poel (1958). Kerner derived the effective properties by relating the average deformation in the inclusion, the matrix and the composite. On the other hand, Van der Poel explicitly considered continuity of displacements and traction between the matrix and the homogeneous material, with the effective composite properties. Later on, Christensen and Lo (1979, 1986) further improved the three-phase model.

The outline of the paper is as follows. In the next section, the boundary value problem of a steadily propagating crack is briefly described. The governing equations are given in Section 3; hydrogen diffusion and hydride-precipitation in Section 3.1 and the elastic deformation of the composite in Section 3.2. With respect to hydride precipitation, in Section 3.1, two cases have been considered: (i) precipitation in a homogeneous medium with the elastic properties of the composite and (ii) precipitation in an inhomogeneous medium, where the expanding hydride has different elastic properties than those of the surrounding solid solution. The differences between the near-tip fields, produced by the above two hydride-precipitation models are discussed in Section 5.1. The effect of remote hydrogen concentration on the near-tip field, when the hydride-precipitation is described by the second model, presented in Section 5.2. Finally, some closing remarks and conclusions are given in Section 6.

2. Boundary value problem

A crack is moving with a constant speed, V_c, under plane strain conditions and constant temperature. A Cartesian coordinate system, (x_1, x_2), with origin at the moving crack tip is considered together with the respective cylindrical coordinate system (r, θ), where the radius r is measured from the crack tip and the angle θ from the crack plane. x_1 is the direction of crack growth.

According to steady-state conditions, an observer, moving with the crack tip, does not see any change in the distribution of a field quantity. Then, a field quantity, q, should only depend on position with respect to the crack tip and not on time, i.e. $q = q(x_1, x_2)$. Consequently, the material time derivative of q satisfies the following well-known relation: $\mathrm{d}q/\mathrm{d}t = -V_c(\partial q/\partial x_1)$.

Far from the crack tip, at a distance which is large compared to the size of the hydride-precipitation zone ahead of the crack tip and along the crack plane, L_{hr}, K-field dominates. Then, the stress tensor, σ_{ij}, is given by the following relation:

$$\sigma_{ij} = \frac{K_I}{\sqrt{2\pi r}} f_{ij}(\theta), \quad r \gg L_{hr}. \tag{1}$$

The italic indices range from one to three. K_I is the mode-I stress intensity factor and f_{ij} is the respective well-known angular stress distribution (e.g. Rice, 1968). Also, far from the crack tip, the concentration of hydrogen, C^H, is constant and equal to C_b^H:

$$C^H = C_b^H, \qquad r \gg L_{hr}. \tag{2}$$

In the present study, where small-scale hydride-precipitation is considered, C_b^H is below the terminal solid solubility of hydrogen in the metal. Note that if hydrides precipitate, far from the crack tip, then K-field does not dominate, under hydrogen chemical equilibrium (Varias, 2003a,b). Indeed, under hydrogen chemical equilibrium, the hydrostatic stress is constant within the hydride-precipitation zone and therefore independent of the distance from the crack tip, r, and the angle from the crack plane, θ.

The remote hydrogen concentration is assumed to be in chemical equilibrium with the hydrogen gas, between the crack faces. The hydrogen gas is also assumed to be in chemical equilibrium with the hydrogen, which is in solid solution on the fracture surface. Therefore, along the crack faces, the following boundary condition is applied:

$$C^H(r,\pm\pi) = C_b^H \exp\left[\frac{\bar{V}^H}{3RT}\sigma_{kk}(r,\pm\pi)\right], \tag{3}$$

where the repeated italic indices denote summation. R, T and $\bar{V}^H$ are the gas constant, the absolute temperature and the molal volume of hydrogen in the solid solution, respectively. It is emphasized that relation (3) does not imply hydrogen chemical equilibrium everywhere in the solid solution. The effect of hydrogen crack face boundary conditions on the near-tip field is discussed by Varias (2003a), where zero hydrogen flux, normal to the crack faces, is also considered. According to theory of partial differential equations, the zero hydrogen flux and the previous relation (3) which are actually corresponding to Neumann and Dirichlet conditions, respectively, must be carefully treated. The reason for this, however, is that Dirichlet conditions are usually forced strongly, whereas Neumann conditions are often enforced weakly, from the view of point of variational principle that is equivalent to Galerkin method. The discontinuous Galerkin formulation concerned with hydrogen-diffusion in metals or alloys, which has a characteristic of local conservation within the frame of element subdomains and is much more available to large-scale computations for convection–diffusion equation, will be reported in our future paper.

Due to symmetry with respect to the crack plane, the shear stress, as well as the displacement and the flux of hydrogen, normal to the crack plane, are zero along the crack line.

3. Governing equations

At constant temperature, delayed hydride cracking results from the simultaneous operation of the processes of hydrogen-diffusion, hydride precipitation and material deformation. The coupling of these processes is taken into account. The model is developed for a metal, M, which forms hydrides of the type MH_x. The presence of the hydrides is described by the hydride volume fraction; the hydrides are smeared. The development of regions rich in hydrides, their shape and size is given by the distribution of hydride volume fraction. Varias (2003a) and Varias and Feng (2004a) give a detailed discussion on the model and the governing equations.

3.1. Hydrogen diffusion and hydride-precipitation

The governing equation of hydrogen-diffusion is the differential form of hydrogen mass conservation, which, under steady-state crack growth conditions, becomes:

$$V_c \frac{\partial C^{HT}}{\partial x_1} = \frac{\partial J_k^H}{\partial x_k}, \tag{4a}$$

$$C^{HT} = fC^{H,hr} + (1-f)C^H, \tag{4b}$$

$$J_k^{\mathrm{H}} = -(1-f)\left(D^{\mathrm{H}}\frac{\partial C^{\mathrm{H}}}{\partial x_k} - \frac{D^{\mathrm{H}}C^{\mathrm{H}}\bar{V}^{\mathrm{H}}}{3RT}\frac{\partial \sigma_{\mathrm{mm}}}{\partial x_k}\right). \tag{4c}$$

The total hydrogen concentration, C^{HT}, is related to the concentration of hydrogen in the solid solution, C^{H}, and the hydride, $C^{\mathrm{H,hr}}$, according to (4b), where f is the volume faction of the hydrides. Note that C^{H} is defined with respect to the volume occupied by the solid solution, i.e. $(1-f)V$. C^{H} is equal to the terminal solid solubility of hydrogen, C^{TS}, when $f \neq 0$. Similarly $C^{\mathrm{H,hr}}$ is defined with respect to the volume occupied by the hydrides, i.e. fV, and therefore it can be considered constant. In relation (4c) of hydrogen flux, J_i^{H}, it was taken into account that hydrogen-diffusion in the hydride is very slow, when compared to the diffusion in the solid solution. In (4c), D^{H} is the diffusion coefficient of hydrogen in the solid solution.

A hydride, MH_x, is assumed to precipitate in the stressed metal under local chemical equilibrium conditions. Consequently:

$$\mu^{\mathrm{hr}} = \mu^{\mathrm{M}} + x\mu^{\mathrm{H}}(C^{\mathrm{TS}}), \tag{5}$$

where μ^{hr}, μ^{M} and μ^{H} are the chemical potentials of the hydride, the metal and hydrogen in the solid solution, under stress, respectively. C^{TS} is the concentration of hydrogen in the solid solution, during the formation of the hydride, and consequently it is equal to the terminal solid solubility of hydrogen in the metal, under stress. Based on (5) one may derive the effect of stress on the terminal solid solubility (Varias and Feng, 2004a):

$$C^{\mathrm{TS}} = C_{\mathrm{e}}^{\mathrm{TS}}\exp\left(\frac{\bar{w}_{\mathrm{int}}}{xRT}\right)\exp\left(\frac{\sigma_{kk}\bar{V}^{\mathrm{H}}}{3RT}\right), \tag{6}$$

where,

$$\bar{w}_{\mathrm{int}} = \bar{w}_1 + \bar{w}_2, \tag{7a}$$

$$\bar{w}_1 = \frac{\kappa^{\mathrm{hr}}}{(\kappa^{\mathrm{M}}-\kappa^{\mathrm{hr}})\alpha - \kappa^{\mathrm{M}}}\cdot\frac{\sigma_{kk}}{3}\theta^{\mathrm{hr}}\bar{V}^{\mathrm{hr}}, \tag{7b}$$

$$\bar{w}_2 = \frac{1}{2}\bar{V}^{\mathrm{hr}}\left[\frac{A}{9\kappa^{\mathrm{M}}}(\sigma_{kk})^2 + \frac{B}{2G^{\mathrm{M}}}\sigma'_{ij}\sigma'_{ij}\right], \tag{7c}$$

$$A = \frac{\kappa^{\mathrm{hr}}-\kappa^{\mathrm{M}}}{(\kappa^{\mathrm{M}}-\kappa^{\mathrm{hr}})\alpha - \kappa^{\mathrm{M}}}, \tag{7d}$$

$$B = \frac{G^{\mathrm{hr}}-G^{\mathrm{M}}}{(G^{\mathrm{M}}-G^{\mathrm{hr}})\beta - G^{\mathrm{M}}}, \tag{7e}$$

$$\alpha = \frac{1}{3}\cdot\frac{1+\nu^{\mathrm{M}}}{1-\nu^{\mathrm{M}}}, \tag{7f}$$

$$\beta = \frac{2}{15}\cdot\frac{4-5\nu^{\mathrm{M}}}{1-\nu^{\mathrm{M}}}. \tag{7g}$$

$C_{\mathrm{e}}^{\mathrm{TS}}$ is the terminal solid solubility of hydrogen, when no external load is applied on the metal, and includes the potential energy for the accommodation of the expanding hydrides. Note that κ^{hr}, G^{hr}, ν^{hr} and κ^{M}, G^{M}, ν^{M} are the bulk modulus, the shear modulus and Poisson's ratio of the hydride and the metal, respectively. θ^{hr} and $\bar{V}^{\mathrm{hr}}$ are the volumetric expansion strain and the molal volume of the hydride phase. Also $\sigma'_{ij}(=\sigma_{ij}-\delta_{ij}\sigma_{kk}/3)$ is the stress deviator. Relations (7a–g) have been derived by assuming that the shape of the hydrides is spherical. Varias and Feng (2004a,b) presented a general relation of hydrogen terminal solid solubility that can take into account elastic modulus difference between hydride and solid

solution, for any hydride shape. Accordingly, interaction energy dealt with this modulus difference is naturally considered also. When the elastic properties of the hydrides and the solid solution are considered to be equal, $\bar{w}_{\text{int}}$ is given by the following relation:

$$\bar{w}_{\text{int}} = -\frac{\sigma_{kk}}{3}\theta^{\text{hr}}\bar{V}^{\text{hr}}. \tag{8}$$

Most of the results, presented in this report, have been derived by using relations (6) and (7a–g), i.e. by considering hydride precipitation in an inhomogeneous medium, where the expanding hydride has different elastic properties than those of the solid solution. Additional calculations have been performed based on relations (6) and (8), i.e. by considering hydride-precipitation in a homogeneous medium with elastic material properties, equal to the effective composite properties. Note that, in both cases, the deformation of the material is calculated by using different hydride and solid solution elastic moduli, according to the composite material model, which is discussed in the following section. The analyses presented in this paper do not attempt to model plastic behavior of hydride coupled with metals, by using composite model. Although plastic hardening/softening rule can be incorporated into elasto-plastic finite element analysis, there is still some debate as to how description of composite material elasto-plasticity should be properly defined. Further research in this area is warranted.

3.2. Material deformation

The material is assumed to be elastic, made of solid solution and hydrides of different stiffness:

$$\sigma_{ij} = D_{ijkl}(\varepsilon_{kl} - \varepsilon^{\text{H}}_{kl}), \tag{9a}$$

$$D_{ijkl} = \lambda\delta_{ij}\delta_{kl} + G(\delta_{ik}\delta_{jl} + \delta_{il}\delta_{jk}), \tag{9b}$$

$$\varepsilon^{\text{H}}_{kl} = \frac{1}{3}\delta_{kl}[f\theta^{\text{hr}} + (1-f)C^{\text{H}}\bar{V}^{\text{H}}]. \tag{9c}$$

ε_{kl}, $\varepsilon^{\text{H}}_{kl}$ are the total strain and the strain caused by hydride formation and hydrogen dissolution, respectively. The elastic coefficients of Lamé, λ and G, correspond to the solid-solution/hydride composite and therefore depend on hydride volume faction.

The coefficients of Lamé are calculated by using a generalized self consistent model (Christensen, 1990; Christensen and Lo, 1979). According to this model, the effective bulk modulus, κ, of the hydride/solid-solution composite is given by the following relation:

$$\kappa = \kappa^{\text{M}} + \frac{f(\kappa^{\text{hr}} - \kappa^{\text{M}})}{1 + (1-f)\dfrac{(\kappa^{\text{hr}} - \kappa^{\text{M}})}{\kappa^{\text{M}} + \frac{4}{3}G^{\text{M}}}}. \tag{10}$$

The effective shear modulus, G, is the positive root of the following second order equation:

$$A_G(G/G^{\text{M}})^2 + 2B_G(G/G^{\text{M}}) + C_G = 0, \tag{11a}$$

where the coefficients are given by:

$$\begin{aligned} A_G = {} & 8\left(\frac{G^{\text{hr}}}{G^{\text{M}}} - 1\right)(4 - 5v^{\text{M}})\eta_1 f^{10/3} - 2\left[63\left(\frac{G^{\text{hr}}}{G^{\text{M}}} - 1\right)\eta_2 + 2\eta_1\eta_3\right]f^{7/3} \\ & + 252\left(\frac{G^{\text{hr}}}{G^{\text{M}}} - 1\right)\eta_2 f^{5/3} - 50\left(\frac{G^{\text{hr}}}{G^{\text{M}}} - 1\right)\left(7 - 12v^{\text{M}} + 8(v^{\text{M}})^2\right)\eta_2 f \\ & + 4(7 - 10v^{\text{M}})\eta_2\eta_3, \end{aligned} \tag{11b}$$

$$B_G = -2\left(\frac{G^{\mathrm{hr}}}{G^{\mathrm{M}}}-1\right)(1-5v^{\mathrm{M}})\eta_1 f^{10/3} + 2\left[63\left(\frac{G^{\mathrm{hr}}}{G^{\mathrm{M}}}-1\right)\eta_2 + 2\eta_1\eta_3\right]f^{7/3} - 252\left(\frac{G^{\mathrm{hr}}}{G^{\mathrm{M}}}-1\right)\eta_2 f^{5/3} + 75\left(\frac{G^{\mathrm{hr}}}{G^{\mathrm{M}}}-1\right)(3-v^{\mathrm{M}})v^{\mathrm{M}}\eta_2 f + \frac{3}{2}(15v^{\mathrm{M}}-7)\eta_2\eta_3, \tag{11c}$$

$$C_G = 4\left(\frac{G^{\mathrm{hr}}}{G^{\mathrm{M}}}-1\right)(5v^{\mathrm{M}}-7)\eta_1 f^{10/3} - 2\left[63\left(\frac{G^{\mathrm{hr}}}{G^{\mathrm{M}}}-1\right)\eta_2 + 2\eta_1\eta_3\right]f^{7/3} + 252\left(\frac{G^{\mathrm{hr}}}{G^{\mathrm{M}}}-1\right)\eta_2 f^{5/3} + 25\left(\frac{G^{\mathrm{hr}}}{G^{\mathrm{M}}}-1\right)[(v^{\mathrm{M}})^2-7]\eta_2 f - (7+5v^{\mathrm{M}})\eta_2\eta_3 \tag{11d}$$

with

$$\eta_1 = \left(\frac{G^{\mathrm{hr}}}{G^{\mathrm{M}}}-1\right)(7-10v^{\mathrm{M}})(7+5v^{\mathrm{hr}}) + 105(v^{\mathrm{hr}}-v^{\mathrm{M}}), \tag{11e}$$

$$\eta_2 = \left(\frac{G^{\mathrm{hr}}}{G^{\mathrm{M}}}-1\right)(7+5v^{\mathrm{hr}}) + 35(1-v^{\mathrm{hr}}), \tag{11f}$$

$$\eta_3 = \left(\frac{G^{\mathrm{hr}}}{G^{\mathrm{M}}}-1\right)(8-10v^{\mathrm{M}}) + 15(1-v^{\mathrm{M}}). \tag{11g}$$

All other elastic moduli of the composite can be calculated by considering the well-known relations for the elastic moduli of isotropic materials.

The coupled problem of hydrogen-diffusion, hydride-precipitation and material deformation is solved numerically by the finite element model, which has been derived from the Galerkin method or variational principle and presented in detail by Varias (2003a,b). However, the global stiffness matrix of the material deformation problem, $K^{\mathrm{op}}_{\mathrm{mn}}$ (see relation (C.9b) of Varias, 2002), is formed and decomposed at every iteration. Indeed, the material deformation global stiffness matrix depends on hydride volume fraction, a quantity, which is also updated at every iteration. Therefore, the running of these calculations usually takes much more time to approach the prescribed converging conditions which must meet to the requirements not only for hydrogen diffusion equation and chemical potential equilibrium, but for governing equations of material deformation as well. One of the promising ways that can significantly speed up the calculation for coupling problem is that pre-conditional conjugate gradient algorithm should be applied.

The general normalized solutions, presented by Varias (2003a,b), however, do not explicitly depend on crack growth velocity, hydrogen diffusion coefficient and temperature. Indeed, by using the normalization $\tilde{x}_i = x_i V_{\mathrm{c}}/D^{\mathrm{H}}$, $\tilde{C}^{\mathrm{H}} = C^{\mathrm{H}}/C^{\mathrm{TS}}_{\mathrm{e}}$ and $\tilde{\sigma}_{ij} = \sigma_{ij}\bar{V}^{\mathrm{H}}/RT$, one derives normalized forms of governing equations, which do not explicitly involve the speed of the crack, the diffusion coefficient of hydrogen and temperature. Consequently, the near tip field, ahead of a steadily propagating crack, has the form $\tilde{u}_i = U_i(\tilde{x}_k;\tilde{K}_{\mathrm{I}},\tilde{C}^{\mathrm{H}}_{\mathrm{b}})$, $\tilde{\sigma}_{ij} = S_{ij}(\tilde{x}_k;\tilde{K}_{\mathrm{I}},\tilde{C}^{\mathrm{H}}_{\mathrm{b}})$, $\tilde{C}^{\mathrm{H}} = C(\tilde{x}_k;\tilde{K}_{\mathrm{I}},\tilde{C}^{\mathrm{H}}_{\mathrm{b}})$, $f = F(\tilde{x}_k;\tilde{K}_{\mathrm{I}},\tilde{C}^{\mathrm{H}}_{\mathrm{b}})$, for displacement, stress, hydrogen concentration and hydride volume fraction, respectively. The displacements have been normalized in the same way as particle coordinates. The near-tip distributions of the normalized quantities depend on the normalized boundary conditions: $\tilde{K}_{\mathrm{I}} = K_{\mathrm{I}}\sqrt{V_{\mathrm{c}}/D^{\mathrm{H}}}/(RT/\bar{V}^{\mathrm{H}})$, which we call the normalized stress intensity factor, and $\tilde{C}^{\mathrm{H}}_{\mathrm{b}} = C^{\mathrm{H}}_{\mathrm{b}}/C^{\mathrm{TS}}_{\mathrm{e}}$. They also depend on normalized material parameters. Note that $D^{\mathrm{H}}/V_{\mathrm{c}}$ is a characteristic length of hydride induced crack growth, related to the size of the area, over which hydrogen redistributes during crack propagation. Also $RT/\bar{V}^{\mathrm{H}}$ is a characteristic stress, introduced by hydrogen-diffusion in relation (4c), which incorporates the effects of temperature and lattice expansion during hydrogen dissolu-

tion. According to the normalized near-tip field, increase of the remote stress intensity factor, K_I, at a given speed, V_c, or increase of the crack tip speed, at a given remote stress intensity factor, leads to similar changes of the near-tip field distributions. Therefore, the study of the normalized near-tip field provides more information near the threshold as well as within stage-II growth.

A quantity, which can also be used for the normalization of stresses, is σ_{kk}^{hr}, i.e. the thermodynamically required constant stress trace within the hydride-precipitation zone, under hydrogen chemical equilibrium. Indeed, according to Varias (2003a,b) and Varias and Feng (2004a), σ_{kk}^{hr} is proportional to RT. Then, at given values of the normalized stress intensity factor, $\tilde{K}_I$, and remote hydrogen concentration, $\tilde{C}_b^H$, D^H/V_c is proportional to $(K_I/\sigma_{kk}^{hr})^2$. Therefore $(K_I/\sigma_{kk}^{hr})^2$ could also be used for normalizing lengths. Note that in an elastic material under hydrogen chemical equilibrium, the extent of the hydride-precipitation zone, ahead of the crack tip and along the crack plane, L_{hr}, is proportional to $(K_I/\sigma_{kk}^{hr})^2$ (Varias, 2003a). For this reason, normalization of lengths by $(K_I/\sigma_{kk}^{hr})^2$ is particularly useful near the threshold stress intensity factor. On the other hand, far from the threshold stress intensity factor and within stage-II growth, the velocity is weakly affected by loading and D^H/V_c is more appropriate for normalizing lengths.

4. Finite element implementation

The solution of the coupled problem of material deformation and hydrogen-diffusion/hydride-precipitation is obtained by iterations, until convergence. Each calculation cycle is divided into two steps, i.e., one step for material deformation and second step for hydrogen-diffusion/hydride-precipitation.

In the case of hydrogen-diffusion and hydride-precipitation, the following equation is derived:

$$\int_V (1-f) D^H C^H \frac{\partial C^H}{\partial x_k} \frac{\partial(\delta C^H)}{\partial x_k} \, dV = \int_{S_\varphi} (C^{HT} V_c n_1 - \varphi^H) \delta C^H \, dS - \int_V V_c C^{HT} \frac{\partial(\delta C^H)}{\partial x_1} \, dV + \int_V (1-f) \frac{D^H C^H \bar{V}^H}{3RT} \frac{\partial \sigma_{mm}}{\partial x_k} \frac{\partial(\delta C^H)}{\partial x_k} \, dV \quad (12)$$

when the governing Eq. (4a) is multiplied, by a variation of hydrogen concentration, δC^H, which is compatible with the boundary conditions, and integrated over a volume, V. S_φ is the part of the bounding surface, where the hydrogen flux is prescribed and equal to $\varphi^H (= J_k^H n_k)$.

With spatial discretization, a system of equations is derived. The solution of this system of equations provides preliminary nodal values of hydrogen concentration in the solid solution. Subsequently, a procedure, similar to that presented by Varias and Massih (2002), is followed for obtaining the new nodal values of the hydride volume fraction and the concentration of hydrogen in solid solution. Note that, when the hydride volume fraction of a node differs from 1 by a specified very small number, the hydrogen concentration in the solid solution of this node is prescribed a value equal to the terminal solid solid solubility.

In the case of material deformation, the algorithm, initially presented by Dean and Hutchinson (1980) and Parks et al. (1981) and subsequently further improved by Varias and Shih (1993, 1994), is employed. In the present application, when the right-hand side vector of the finite element equation is calculated, the contribution of the hydrogen/hydride-induced expansion strain is also included. Also the global stiffness matrix of the material deformation problem is formed and decomposed at every calculation cycle. Indeed the material deformation global stiffness matrix depends on hydride volume fraction, a quantity, which also is updated at every calculation cycle.

5. Discussion of results

The results of the present simulations correspond to crack growth in Zircaloy-2 at 300 °C, due to the precipitation and fracture of δ-hydrides. The properties of the materials are given in Table 1, together with

Table 1
Material properties used in the finite element calculations. The material properties correspond to Zircaloy-2 and δ-hydride ($ZrH_{1.66}$)

E^{M}, ν^{M}	80.4 GPa, 0.369 (573 K)	Wäppling et al. (1998)
E^{hr}, ν^{hr}	135.9 GPa, 0.32	Kuroda et al. (2000)
D^{H}	$2.17\times10^{-7}\exp(-35087.06/RT)$ m^2/s	Sawatzky (1960)
C_e^{TS}	$6.3741\times10^{5}\exp(-34542.75/RT)$ mol/m^3	Kearns (1967)
$C^{H,hr}$	1.02×10^{5} mol/m^3	Varias and Massih (2002)
$\bar{V}^{H}$	7×10^{-7} m^3/mol	Dutton et al. (1977)
$\bar{V}^{hr}$	16.3×10^{-6} m^3/mol	Puls (1984)
θ^{hr}	0.1636	Varias and Massih (2002)
x	1.66	δ-hydride, ZrH_x (e.g. Puls, 1984)

The source of information is included.

the source of the information. In the stress distributions, stresses have been normalized by the thermodynamically required stress trace in the hydride-precipitation zone, under hydrogen chemical equilibrium, $\sigma_{kk}^{hr} \cong (3x/\theta^{hr}\bar{V}^{hr})RT\ln(C_e^{TS}/C_b^{H})$, (Varias, 2002, relation (22b); Varias, 2003a). This relation has been derived, by considering precipitation in a homogeneous material, i.e. by using relations (6) and (8) for hydrogen terminal solid solubility.

5.1. Comparison of the composite material models

The predictions of the two composite models have been compared for a wide range of the normalized stress intensity factor, corresponding to crack growth from stage-I, near the threshold stress intensity factor, to stage-II.

Fig. 1a shows the distributions of the normalized stress trace, ahead of the crack tip and along the crack plane, derived by both composite models, near the threshold stress intensity factor. Distances have been normalized by $(K_I/\sigma_{kk}^{hr})^2$. Note that for $\tilde{K}_I = 0.0013$ and an applied stress intensity factor, K_I, about equal to 10 MPa $\sqrt{m}$, the crack growth velocity is 10^{-10} m/s. Therefore it is confirmed that Fig. 1 shows the stress distribution near threshold and crack arrest. The calculations have been performed for a remote hydrogen concentration near the terminal solid solubility, i.e. for $\tilde{C}_b^{H}$ about equal to 0.94, which corresponds to σ_{kk}^{hr} equal to 580 MPa, according to relation (22) of Varias and Feng (2004a). The difference between the stress trace distributions of the two composite models is almost negligible far from the crack tip, in the solid solution. Both models predict the development of the stress plateau, within the hydride-precipitation zone. The stress trace level, for the composite model, based on (8), is in agreement with relation (22) of Varias and Feng (2004a). On the other hand, the stress trace level, for the composite model, based on (7a–g), is in agreement with relation (23) of Varias and Feng (2004a), which takes into account the different hydride and solid solution elastic properties. Note that the difference between the two stress levels, given by relations (22b) and (23), is only 5.2%. The difference between the two models becomes significant only very close to the crack tip for an appreciable hydride volume fraction (see Fig. 2a), for which deviation from the stress plateau is also observed. Indeed, the stress plateau is thermodynamically required only within the solid solution of the hydride-precipitation zone. Then, when the hydride volume fraction becomes appreciable, the overall stress trace in the hydride/solid-solution composite deviates from that required by hydrogen chemical equilibrium. It should also be mentioned that the stress distribution of the composite model, based on (8), is nearly the same as that predicted by considering identical hydride and solid solution elastic properties for the material deformation too (compare Fig. 1a, in the present work, with Fig. 7a of Varias and Feng, 2004a). Fig. 1b provides the distributions of the hoop stress ahead of the crack tip and along the crack plane, produced by the two composite models for $\tilde{K}_I = 0.0013$ and $\tilde{C}_b^{H} = 0.94$; the hoop stress is responsible for the fracture of the near-tip hydrides and consequently for the propagation of the crack. These distributions are nearly identical. Nearly identical are also the respective distributions of

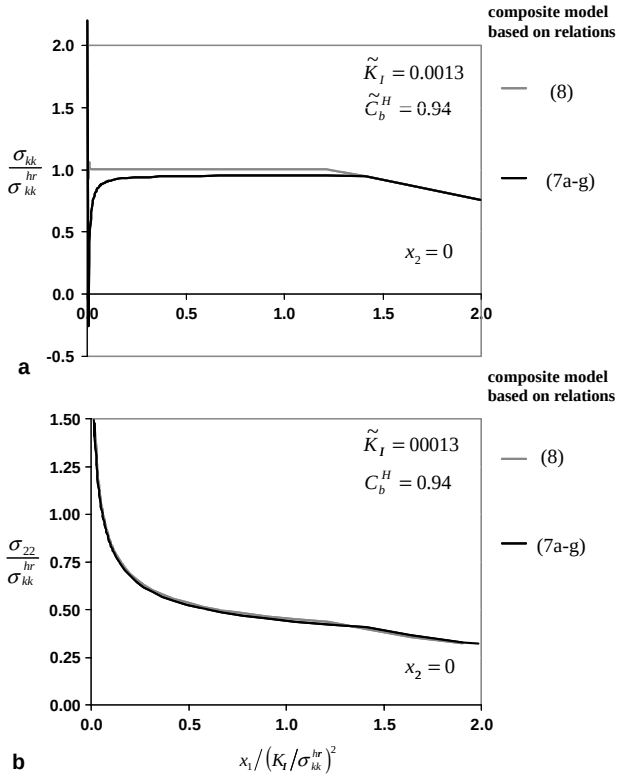

Fig. 1. Normalized distributions of (a) stress trace and (b) hoop stress, on the crack plane, for the two composite models. The distributions correspond to relatively small crack velocities, when hydrogen chemical equilibrium is approached.

the hydride volume fraction, in Fig. 2a, as well as of Lamé coefficients, λ and G, in Fig. 2b. According to Fig. 2a, the normalized size of the hydride-precipitation zone, ahead of the crack tip, $L_{\rm hr}/(K_{\rm I}/\sigma_{kk}^{\rm hr})^2$, is equal to 1.21, i.e., only by 1.4% different from the theoretical prediction of relation (25), given by Varias and Feng (2004a). The coefficients of Lamé have been normalized by the respective values of the solid solution. Therefore, they vary from 1, far from the crack tip, to $\lambda^{\rm hr}/\lambda^{\rm M}$ and $G^{\rm hr}/G^{\rm M}$ as the crack tip is approached.

Figs. 3a, b and 4a, b show the distributions, ahead of the crack tip on the crack plane, of stress trace, hoop stress, hydride volume fraction and Lamé coefficients, respectively, derived by both composite models, for $\tilde{K}_{\rm I} = 0.0422$ and $\tilde{C}_{\rm b}^{\rm H} = 0.94$. Note that, when $K_{\rm I}$, is about equal to 10 MPa $\sqrt{\rm m}$, the crack growth velocity is 10^{-7} m/s. Therefore the distributions in Figs. 3 and 4 correspond to conditions far from hydrogen chemical equilibrium, when the crack propagates in the transition between stages-I and II regimes. Distances have been normalized by $D^{\rm H}/V_{\rm c}$. The fields, which are predicted by the two composite models, differ negligibly. Negligible are also the differences between the distributions of field quantities, derived by the two composite models, for larger values of the normalized stress intensity factor, when the crack propagates within the stage-II regime. In this case, both composite models predict distributions, which are nearly identical to those derived by a homogeneous material model, where the hydride elastic properties are equal to those of the solid solution (e.g. see Fig. 10 of Varias and Feng, 2004a).

It is argued that elastic modulus difference between hydride and solid solution, under steady-state crack propagation, only affects apparently near crack-tip the distributions of field quantities, through the previous comparisons.

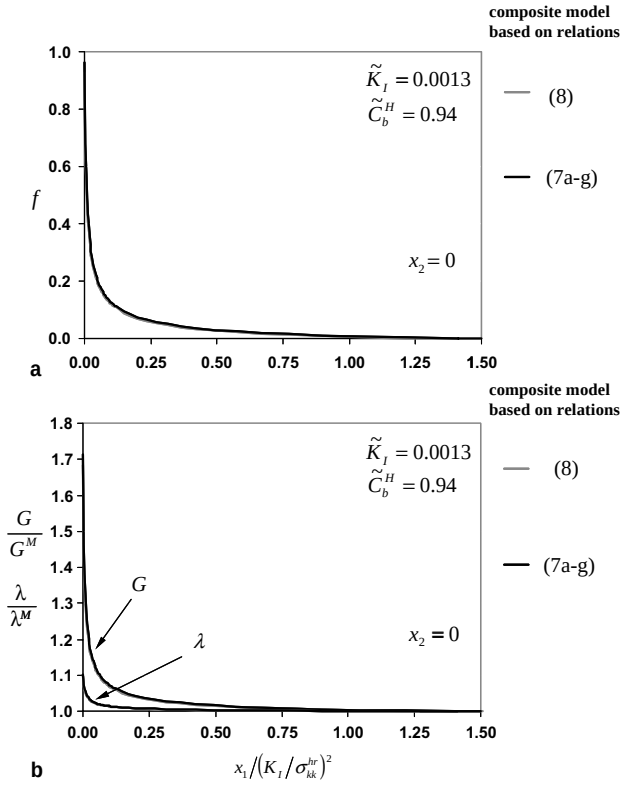

Fig. 2. Normalized distributions of (a) hydride volume fraction and (b) Lamé coefficients of the hydride/solid-solution composite, on the crack plane, derived by the two composite models. The distributions correspond to relatively small crack velocities, when hydrogen chemical equilibrium is approached.

5.2. Effect of remote hydrogen concentration on near-tip field

In the present section, the results have been derived, by using only the inhomogeneous material model for hydride-precipitation, which is based on relations (7a–g). The effect of remote hydrogen concentration on the near-tip field is discussed for $0.0013 \leqslant \tilde{K}_{\mathrm{I}} \leqslant 0.1334$, which corresponds to a wide range of crack growth conditions, from stage-I to stage-II.

When the normalized stress intensity factor is very small, corresponding to small values of the crack velocity, hydrogen chemical equilibrium is approached, irrespectively of the level of hydrogen concentration far from the crack tip. Then, chemical equilibrium controls the distribution of stresses, in the zone of hydride-precipitation, and therefore the effect of remote hydrogen concentration, on normalized distributions, is expected to be weak. Indeed, Fig. 5a and b, which show the distributions of the stress trace and the hoop stress, on the crack plane, for $\tilde{K}_{\mathrm{I}} = 0.0013$ and $\tilde{C}_{\mathrm{b}}^{\mathrm{H}} = 0.94$, 0.70 and 0.30, confirm the above reasoning. Distances have been normalized by $(K_{\mathrm{I}}/\sigma_{kk}^{\mathrm{hr}})^2$ and therefore the area of hydride-precipitation extents over a normalized length of about 1.20. In Fig. 5a, the stress trace plateau develops, clearly, in the hydride-precipitation zone, for all cases of remote hydrogen concentration. Note that the stress has been normalized by $\sigma_{kk}^{\mathrm{hr}}$, which is proportional to $\ln(1/1\tilde{C}_{\mathrm{b}}^{\mathrm{H}})$. and therefore varies significantly with $\tilde{C}_{\mathrm{b}}^{\mathrm{H}}$. Then as $\tilde{C}_{\mathrm{b}}^{\mathrm{H}}$ changes from 0.94 to 0.70 or 0.30, $\sigma_{kk}^{\mathrm{hr}}$ increases 5.8 times or 19.5 times, respectively. Consequently, the actual values of the stresses increase as $\tilde{C}_{\mathrm{b}}^{\mathrm{H}}$ decreases from 0.94 to 0.70 or 0.30. The effect of $\tilde{C}_{\mathrm{b}}^{\mathrm{H}}$, on the normalized stress

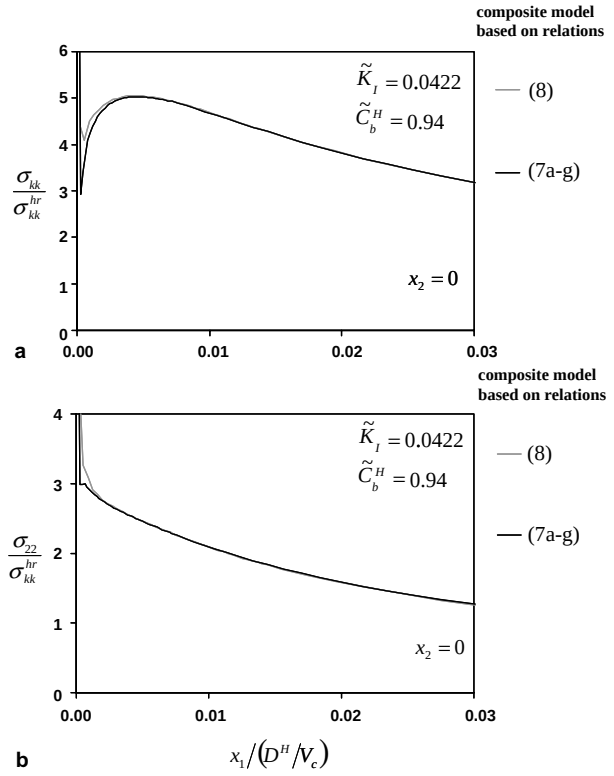

Fig. 3. Normalized distributions of (a) stress trace and (b) hoop stress, on the crack plane, for the two composite models. The distributions correspond to conditions of crack growth, within the transition from stages-I to II regime, far from hydrogen chemical equilibrium.

distribution, becomes important, very close to the crack tip, where the hydride volume fraction is appreciable and leads to deviation from the thermodynamically required stress trace. In the same region, the normalized hoop stress is also affected by the hydrogen content, far from the crack tip, (Fig. 5b).

Fig. 6 presents the distributions of hydride volume fraction, on the crack plane, for $\tilde{K}_{\mathrm{I}} = 0.0013$ and $\tilde{C}_{\mathrm{b}}^{\mathrm{H}} = 0.94$, 0.70 and 0.30. Note again that distances have been normalized by $(K_{\mathrm{I}}/\sigma_{kk}^{\mathrm{hr}})^2$. Taking into account the significant variation of $\sigma_{kk}^{\mathrm{hr}}$ with $\tilde{C}_{\mathrm{b}}^{\mathrm{H}}$ and the distributions of Fig. 6, one concludes that the hydride volume fraction, actually, increases with the increase of the remote hydrogen concentration. This is observed, when a certain not normalized distance from the crack tip is considered, for a given value of the applied stress intensity factor. Similarly, for a given value of the applied stress intensity factor, the actual size of the hydride-precipitation zone increases with the remote hydrogen concentration that can be confirmed from Fig. 10 as well.

The hydride volume fraction controls the variation of the elastic properties of the hydride/solid-solution composite. Indeed, the distributions of Lamé coefficients of the composite, shown ahead of the crack tip and along the crack plane in Fig. 7, are similar to those of the hydride volume fraction.

When the normalized stress intensity factor corresponds generally to conditions, which deviate from hydrogen chemical equilibrium, the effect of remote hydrogen concentration on the normalized near tip field is strong. Fig. 8a and b show the distributions, on the crack plane, of the stress trace and the hoop stress, respectively, for $\tilde{K}_{\mathrm{I}} = 0.0422$ and $\tilde{C}_{\mathrm{b}}^{\mathrm{H}} = 0.94$, 0.70 and 0.30. Distances have been normalized by

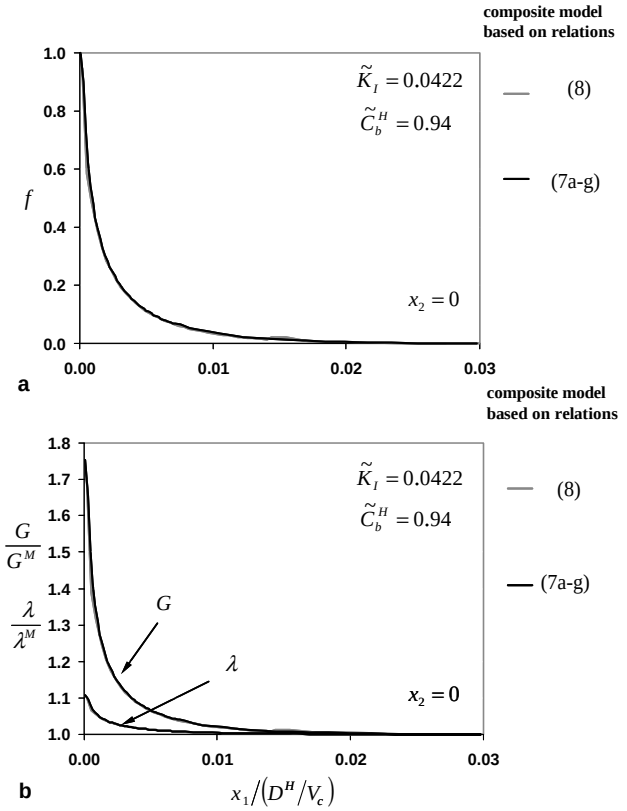

Fig. 4. Normalized distributions of (a) hydride volume fraction and (b) Lamé coefficients of the hydride/solid-solution composite, on the crack plane, derived by the two composite models. The distributions correspond to conditions of crack growth, within the transition from stage-I to stage-II regime, far from hydrogen chemical equilibrium.

D^H/V_c. The stresses have also been normalized by σ_{kk}^{hr}. Taking into account the variation of σ_{kk}^{hr} with $\tilde{C}_b^H$ one concludes that the actual values of the stresses increase as $\tilde{C}_b^H$ decreases from 0.94 to 0.70 or 0.30. According to Fig. 8a, for the remote hydrogen concentration close to the terminal solid solubility, $\tilde{C}_b^H = 0.94$, the stress trace deviates significantly from the thermodynamically required value, under hydrogen chemical equilibrium. However, as $\tilde{C}_b^H$ decreases, the stress trace, near the crack tip, tends to σ_{kk}^{hr}. Indeed, for $\tilde{C}_b^H = 0.30$ a stress plateau develops ahead of the crack tip. This is more clearly shown in Fig. 9, where the distributions for (i) $\tilde{K}_I = 0.0422/C_b^H = 0.30$ and (ii) $\tilde{K}_I = 0.0013/C_b^H = 0.94$ are compared. Note that for a given value of the applied stress intensity factor, K_I, the distribution in case (i) corresponds to a crack velocity 1000 times larger than that of case (ii). Therefore, reduction of remote hydrogen concentration leads to distributions closer to those under hydrogen chemical equilibrium, a trend, which is also produced by reduction of the crack tip velocity and the applied stress intensity factor.

Fig. 10 shows the hydride volume fraction distribution on the crack plane for $\tilde{K}_I = 0.0422$ and $\tilde{C}_b^H = 0.94$, 0.70 and 0.30. In this case, distances have been normalized by D^H/V_c, and therefore it is clearly shown that the hydride-precipitation zone increases with the increase of the remote hydrogen concentration, assuming that in all three cases the velocity of the crack is the same.

Further increase of the normalized stress intensity factor to values, corresponding to stage-II growth, does not change the trends shown in Fig. 8. Indeed, Fig. 11 presents the distributions, on the crack plane,

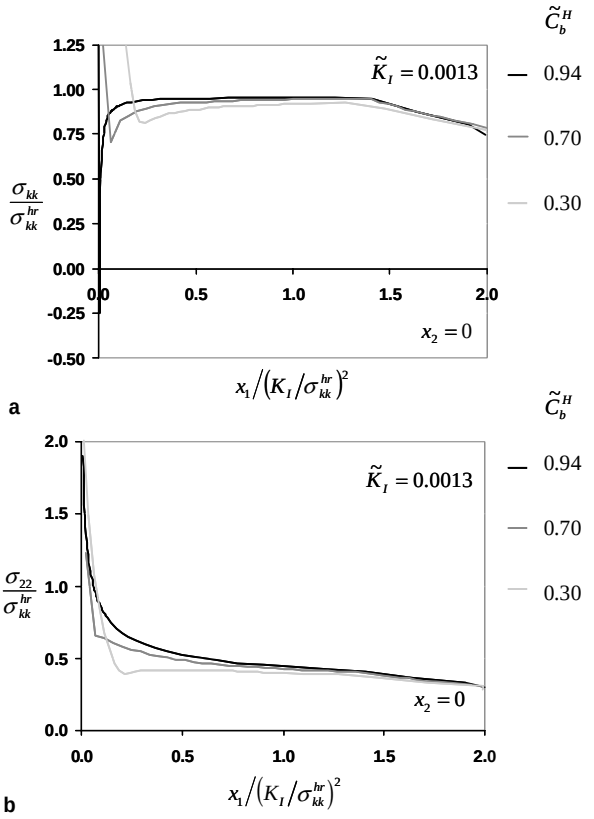

Fig. 5. Normalized distributions of (a) stress trace and (b) hoop stress, on the crack plane, for different values of remote hydrogen concentration, based on inhomogeneous hydride-precipitation, i.e. relations (7a–g). The distributions correspond to relatively small crack velocities, when hydrogen chemical equilibrium is approached.

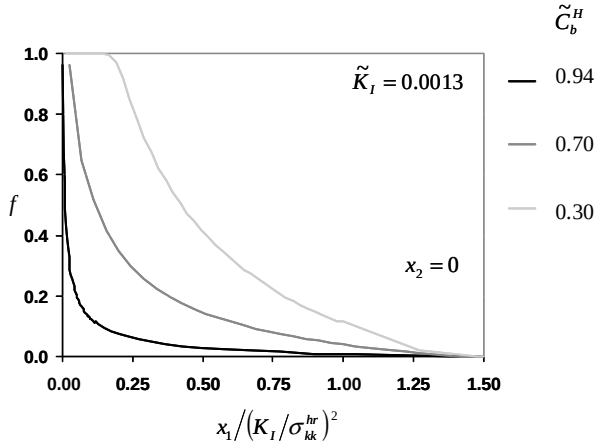

Fig. 6. Normalized distributions of hydride volume fraction, on the crack plane, for different values of remote hydrogen concentration, based on inhomogeneous hydride-precipitation, i.e. relations (7a–g). The distributions correspond to relatively small crack velocities, when hydrogen chemical equilibrium is approached.

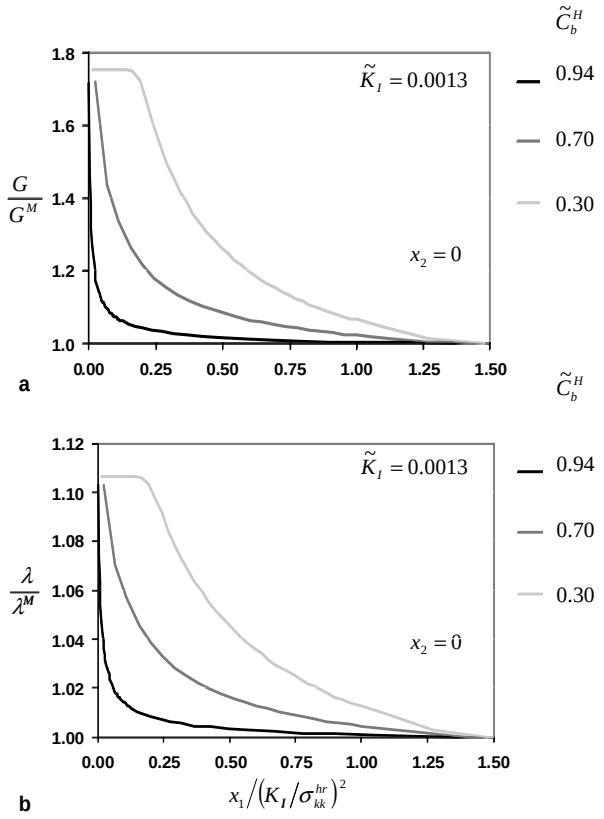

Fig. 7. Normalized distributions of the coefficients of Lamé for the hydride/solid-solution composite, on the crack plane, under different values of remote hydrogen concentration. Inhomogeneous hydride precipitation, i.e. relations (7a–g), has been considered. The distributions correspond to relatively small crack velocities, when hydrogen chemical equilibrium is approached.

of the stress trace and the hoop stress, for $\tilde{K}_{\mathrm{I}} = 0.1334$ and $\tilde{C}_{\mathrm{b}}^{\mathrm{H}} = 0.94$, 0.70 and 0.30. For a given value of the applied stress intensity factor, the distributions of Fig. 11 correspond to a crack velocity 10 times larger than that in Fig. 8. The strong effect of the remote hydrogen concentration, on the normalized distributions, is again shown. Again increase of $\tilde{C}_{\mathrm{b}}^{\mathrm{H}}$ leads to larger values of the normalized stresses, $\sigma_{ij}/\sigma_{kk}^{\mathrm{hr}}$.

6. Closing remarks and conclusions

The composite material model applied to analyze the coupling effects of temperature, hydride and metal elastic properties, under steady-state crack condition, has been shown to be a reliable and robust model for assessing the distributions of stresses, the values of hydride volume fraction, and the distributions of hydrogen concentration. It must be emphasized that interaction energy induced by elastic modulus difference has been properly reflected in the relation of terminal solid solubility. It is notable that the hydrostatic stress plateau level and even hydride volume fraction are all completely agreed with the previous evaluation, which regarded hydride and solid solution as an identical elastic material (Varias and Feng, 2004a,b).

The material is assumed to be an elastic composite made of hydrides and solid solution, with properties depending locally on the volume fraction of the hydrides. In the present analysis, the composite elastic

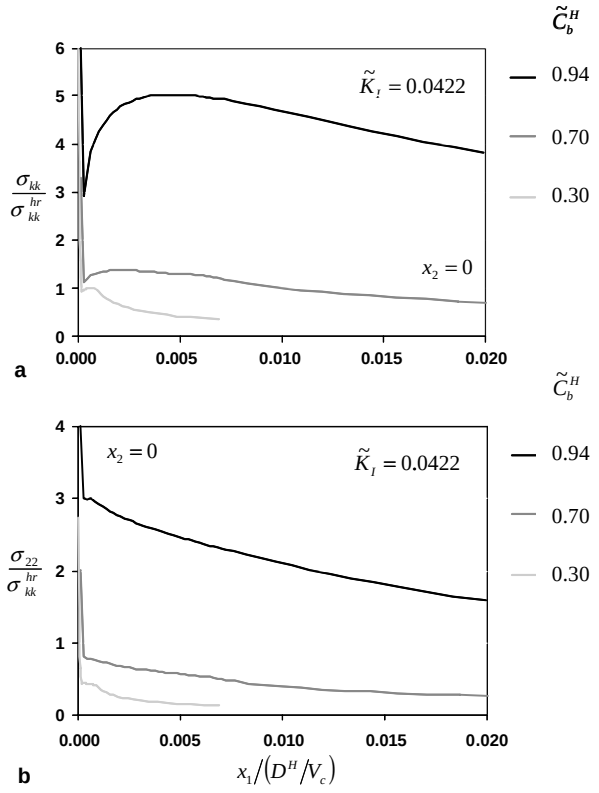

Fig. 8. Normalized distributions of (a) stress trace and (b) hoop stress, on the crack plane, for different values of remote hydrogen concentration, based on inhomogeneous hydride-precipitation, i.e. relations (7a–g). For $\tilde{C}_b^H = 0.94$, the distributions correspond to conditions, far from hydrogen chemical equilibrium, in the transition from stage-I to stage-II regime.

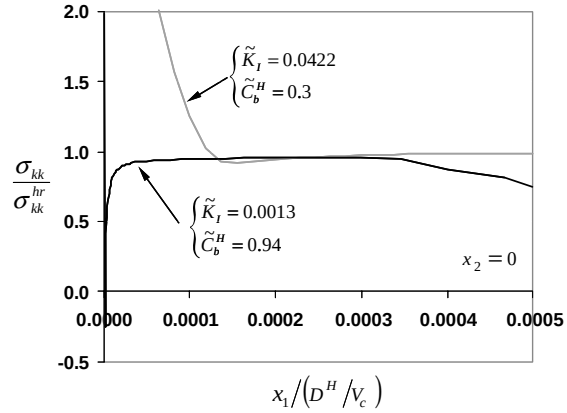

Fig. 9. Normalized distributions of the stress trace, on the crack plane, for two different cases of normalized stress intensity factor and remote hydrogen concentration. Inhomogeneous hydride-precipitation, i.e. relations (7a–g), has been considered. Both distributions approach hydrogen chemical equilibrium.

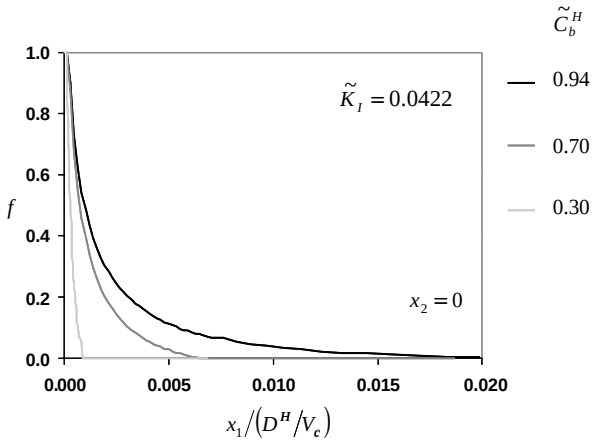

Fig. 10. Normalized distributions of hydride volume fraction, on the crack plane, for different values of remote hydrogen concentration, based on inhomogeneous hydride-precipitation, i.e. relations (7a–g). For $\tilde{C}_b^H = 0.94$, the distribution corresponds to conditions, far from hydrogen chemical equilibrium, in the transition from stage-I to stage-II regime.

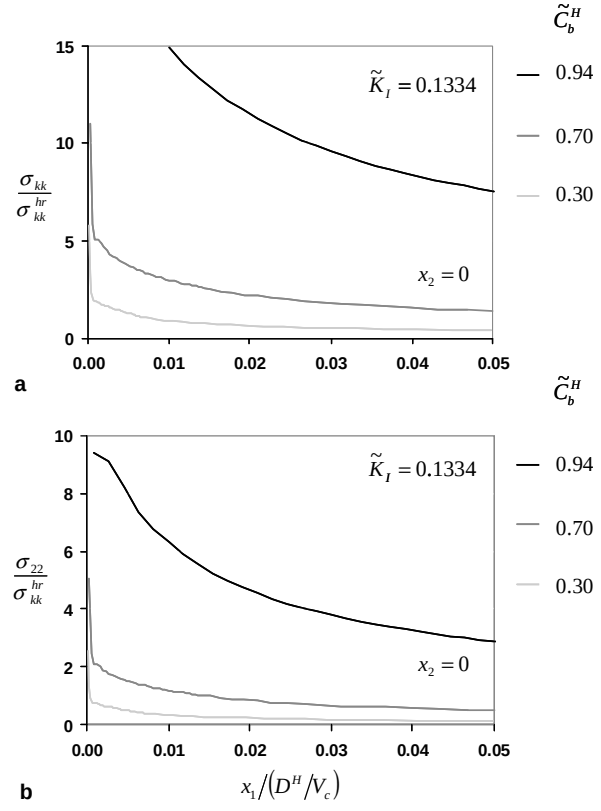

Fig. 11. Normalized distributions of (a) stress trace and (b) hoop stress, on the crack plane, for different values of remote hydrogen concentration, based on inhomogeneous hydride-precipitation, i.e. relations (7a–g). The distributions correspond to conditions, far from hydrogen chemical equilibrium.

properties have been derived by a generalized self consistent model for particulate composites. Hydride precipitation is also predicted by using a relation of hydrogen terminal solid solubility, which takes into account the different elastic properties of the solid solution and hydride phases.

The effect of the hydrogen concentration far from the crack tip, on the near-tip field, is studied. It is shown that for small crack growth velocities, near the threshold stress intensity factor, the remote hydrogen concentration weakly influences the normalized stress distribution in the hydride-precipitation zone, which is controlled by the thermodynamically required constant hydrostatic stress under hydrogen chemical equilibrium. However, for values of the applied stress intensity factor and of the crack tip velocity away from the threshold stress intensity factor and crack arrest, the effect of remote hydrogen concentration on the normalized near-tip stress field is strong. Reduction of the remote hydrogen concentration generally leads to reduction of the hydride-precipitation zone and increase of the near-tip stresses. Also reduction of the remote hydrogen concentration leads to distributions closer to those under hydrogen chemical equilibrium.

Acknowledgements

The present study is part of the project on 'Hydrogen Embrittlement and Fracture in Hydride Forming Metals', which is financed by the Foundation for Knowledge and Competence Development (Project Grant Hög 2000, KK-Stiftelsen, Sweden). The project is performed with the cooperation of Studsvik Nuclear AB and Barsebäck Kraft AB. The work of J.L.F. was partly supported by the special fund of Beijing University of Technology as well.

References

Budiansky, B., 1965. On the elastic moduli of some heterogeneous materials. Journal of the Mechanics and Physics of Solids 13, 223.

Christensen, R.M., 1990. A critical evaluation for a class of micro-mechanics models. Journal of the Mechanics and Physics of Solids 38, 379–404.

Christensen, R.M., 1979. Mechanics of Composite Materials. John Wiley & Sons, New York.

Christensen, R.M., Lo, K.H., 1979. Solutions for effective shear properties in three phase sphere and cylinder models. Journal of the Mechanics and Physics of Solids 27, 315–330.

Christensen, R.M., Lo, K.H., 1986. Erratum. Journal of the Mechanics and Physics of Solids 34, 639.

Dean, R.H., Hutchinson, J.W., 1980. Quasi-Static steady crack growth in small scale yielding. In: Fracture Mechanics. Twelfth Conference, ASTM STP 700. American Society for Testing of Materials, Philadelphia, PA, pp. 383–405.

Dutton, R., Nuttall, K., Puls, M.P., Simpson, L.A., 1977. Mechanisms of hydrogen induced delayed cracking in hydride forming materials. Metallurgical Transactions A 8A, 1553–1562.

Efsing, P., 1998. Delayed hydride cracking in irradiated zircaloy, Ph.D. Thesis, Royal Institute of Technology, Stockholm, Sweden.

Hashin, Z., 1962. The elastic moduli of heterogeneous materials. Journal of Applied Mechanics 29, 143–150.

Hill, R., 1965. A self-consistent mechanics of composite materials. Journal of the Mechanics and Physics of Solids 13, 213.

Kearns, J.J., 1967. Terminal solubility and partitioning of hydrogen in the alpha phase of zirconium, zircaloy-2 and zircaloy-4. Journal of Nuclear Materials 22, 292–303.

Kerner, E.H., 1956. The elastic and thermoelastic properties of composite media. Proceedings of Physics Society 69, 808.

Kuroda, M., Yoshioka, K., Yamanaka, S., Anada, H., Nagase, F., Uetsuka, H., 2000. Influence of precipitated hydride on the fracture behavior of zircaloy fuel cladding tube. Journal Nuclear and Science and Technology 37, 670–675.

Lufrano, J., Sofronis, P., Birnbaum, H.K., 1998. Elasto-plastically accommodated hydride formation and embrittlement. Journal of the Mechanics and Physics of Solids 46, 1497–1520.

Lufrano, J., Sofronis, P., Birnbaum, H.K., 1996. Modeling of hydrogen transport and elastically accommodated hydride formation near a crack tip. Journal of the Mechanics and Physics of Solids 44, 179–205.

Northwood, D.O., Kosasih, U., 1983. Hydrides and delayed hydrogen cracking in zirconium and its alloys. International Metals Reviews 28, 92–121.

Parks, D.M., Lam, P.S., McMeeking, R.M., 1981. Some Effects of inelastic constitutive models on crack tip fields in steady quasistatic growth. In: Francois, D., (Ed.), Advances in Fracture Research. 5th International Conference on Fracture, Cannes, vol. 5. pp. 2607–2614.

Puls, M.P., 1984. Elastic and plastic accommodation effects on metal-hydride solubility. Acta Metallurgica 32, 1259–1269.
Rice, J.R., 1968. Mathematical analysis in the mechanics of fracture. In: Liebowitz, H. (Ed.), Fracture: An Advanced Treatise, vol. II. Academic Press, New York, pp. 191–311.
Sawatzky, A., 1960. Hydrogen in zircaloy-2: its distribution and heat of transport. Journal of Nuclear Materials 2, 321–328.
Serebrinsky, S., Carter, E.A., Ortiz, M., 2004. A quantum-mechanically informed continuum model of hydrogen embrittlement. Journal of the Mechanics and Physics of Solids 52, 2403–2430.
Soforonis, P., 2001. Recent advances in the engineering aspects of hydrogen embrittlement—Special number. Engineering and Fracture Mechanics 68 (6), 617–837.
Taha, A., Soforonis, P., 2001. A micromechanics approach to the study of hydrogen transport and embrittlement. Engineering and Fracture Mechanics 68 (6), 803–837.
Torquato, S., 1997. Exact expression for the effective elastic tensor of disordered composite. Physical Review Letters 79 (4), 681–684.
Van der Poel, C., 1958. On the rheology of concentrated dispersions. Rheologica Acta 1 (1), 198.
Varias, A.G., 1998. Mathematical Model for Hydrogen Diffusion, Energy Flow and Hydride Formation in Zirconium under stress. Report BR-04-10-98, Solid Mechanics Research Office, Athens, Greece.
Varias, A.G., 2002. Steady-State Crack Growth due to Hydride-Induced Embrittlement Effect of Hydride Precipitation on Near-tip Hydrostatic Stress. Report PA-01-06-02, Malmö University, Malmö, Sweden.
Varias, A.G., 2003a. Hydrogen embrittlement and sub-critical crack growth in hydride forming metals. In: Proceedings of the 5th Euromech Solid Mechanics Conference (ESMC), Thessaloniki, Greece.
Varias, A.G., 2003b. Hydride-induced steady-state crack growth in metals. In: Proceedings of the 9th International Conference on the Mechanical Behaviour of Materials, Geneva, Switzerland.
Varias, A.G., Feng, J.L., 2004a. Simulation of hydride-induced steady-state crack growth in metals. Part I: Growth near hydrogen chemical equilibrium. Computational Mechanics 34 (5), 335–356.
Varias, A.G., Feng, J.L., 2004b. Simulation of hydride-induced steady-state crack growth in metals. Part II: General near tip field. Computational Mechanics 34 (5), 357–376.
Varias, A.G., Massih, A.R., 2000. Simulation of hydrogen embrittlement in zirconium alloys under stress and temperature gradients. Journal of Nuclear Materials 279, 273–285.
Varias, A.G., Massih, A.R., 2002. Hydride-induced embrittlement and fracture in metals effect of stress and temperature distribution. Journal of the Mechanics and Physics of Solids 50, 1469–1510.
Varias, A.G., Shih, C.F., 1993. Quasi-static crack advance under a range of constraints steady-state fields based on a characteristic length. Journal of the Mechanics and Physics of Solids 41, 835–861.
Varias, A.G., Shih, C.F., 1994. Dynamic steady crack growth in elastic–plastic solids propagation of strong discontinuities. Journal of the Mechanics and Physics of Solids 42, 1817–1848.
Wäppling, D., Massih, A.R., Ståhle, P., 1998. A model for hydride-induced embrittlement in zirconium-based alloys. Journal of Nuclear Materials 249, 231–238.